Ultranarrow Band Absorbers Based on Surface Lattice Resonances in Nanostructured Metal Surfaces

Zhongyang Li, Serkan Butun, and Koray Aydin*

Department of Electrical Engineering and Computer Science, Northwestern University, Evanston, Illinois 60208, United States

ABSTRACT Nanostructured metals have received a significant amount of attention in recent years due to their exciting plasmonic and photonic properties enabling strong field localization, light concentration, and strong absorption and scattering at their resonance frequencies. Resonant plasmonic and metamaterial absorbers are of particular interest for applications in a wide variety of technologies including photothermal therapy, thermophotovoltaics, heat-assisted magnetic recording, hot-electron collection, and biosensing. However, it is rather challenging to realize ultranarrow absorption bands using plasmonic materials due to large optical losses in metals that decrease the quality factor of optical resonators. Here, we theoretically and experimentally demonstrate an ultranarrow band absorber based on the surface lattice resonances (SLRs) in periodic nanowire and nanoring arrays on optically thick, reflecting metallic films. In experiments, we observed ultranarrow band resonant absorption peaks with a bandwidth of 12 nm and absorption amplitude exceeding 90% at visible frequencies. We demonstrate that the resonance absorption wavelength, amplitude of the absorption peak, and the bandwidth can be controlled by tuning the periodicity and the thickness of nanoring and nanowire arrays. Unlike conventional plasmonic absorbers utilizing common metal–insulator–metal stacks, our narrow band absorber consists solely of metals, facilitating stronger optical interaction between the SLR of periodic nanostructures and the highly reflective film. Moreover, by introducing asymmetry to the nanoring/nanowire hybrid system, we observe the spectral evolution of resonance splitting enabled by strong coupling between two individual SLRs arising from nanoring and nanowire arrays. Designing such all-metallic nanostructure arrays is a promising route for achieving ultranarrow band absorbers which can be used as absorption filters, narrow band thermal emitters in thermophotovoltaics, and plasmonic biosensors.

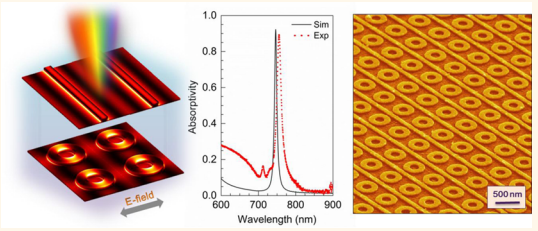

KEYWORDS: plasmonics · narrow band · perfect absorption · surface lattice resonance · nanostructures · ultrasensitive biosensing · symmetry breaking

Resonant plasmonic and metamaterial structures allow many exciting optical phenomena, from optical negative refraction[1,2] and perfect lensing[3,4] to optical cloaking,[5] and enable novel or enhanced functionalities in various devices, such as photonic modulators,[6,7] optical filters,[8] biosensors,[9–12] and broad-band super absorbers.[13,14] Most of these applications greatly benefit from unique properties of metals supporting strong localized or propagating plasmon resonance modes that can be controlled by the size, geometry, and optical properties of the plasmonic material and surrounding dielectric medium. One of the criticisms for using metals in optical applications has been the inherent optical losses of metals. However, recently, optical losses in plasmonic materials has been utilized for enhancing light absorption through optical resonances that can find use in photothermal therapy,[15] thermophotovoltaics,[13] heat-assisted magnetic recording,[16] hot-electron collection,[17] thermal emission,[18] biosensing applications,[19] and solar-steam generation.[20] Triple-layer metal–insulator–metal (MIM) film stacks have been a common and standard design in previous plasmonic and metamaterial absorber designs,[13,21,22] where the size and the periodicity of top metal nanostructures and the dielectric spacer thickness control both the localized and delocalized surface plasmon resonance wavelengths. Eventually, incident light gets absorbed due to strong optical interaction around the resonant wavelengths and converted to heat in lossy metallic sections. The resonance bandwidth of plasmonic absorbers is relatively broad (>40 nm), and it is rather

* Address correspondence to aydin@northwestern.edu.

Received for review May 13, 2014 and accepted July 29, 2014.

Published online July 29, 2014
10.1021/nn502617t

challenging to design ultranarrow plasmonic absorbers due to high optical losses in metals, which significantly decrease the quality factor of plasmonic resonators.

In this article, we propose and demonstrate ultranarrow band absorbers based on the surface lattice resonances[23] (SLRs) of nanoring and nanowire arrays on optically thick metallic films. Here, we report the results from our theoretical and experimental study, in which we realized a narrow band absorber (NBA) with an absorption bandwidth of 12 nm and absorptivity exceeding 90%. Metal nanostructures fabricated on metallic films not only excite sharp absorption resonances[24] but also facilitate much stronger electric field localization at the top metal/air interface. The physical mechanism behind our proposed all-metal narrow band absorber is the SLR, which is essentially an intricate combination of localized/delocalized surface plasmon resonances on diffractive orders in periodic arrays.

RESULTS AND DISCUSSION

All-Metallic Nanowire and Nanoring Arrays. Our narrow band absorber design is based on periodic arrays of gold nanowires (Figure 1a), nanorings (Figure 1b), and a combination of nanowires and nanorings (Figure 1c) that are fabricated on top of an optically thick gold film using electron beam (E-beam) lithography. The thickness of gold nanostructures is $h = 40$ nm, and the lattice constant is $p = 700$ nm. The width of the nanowire is $a = 100$ nm, and the inner radius and width of the nanoring is $r = 100$ nm and $w = 140$ nm. The gold film is optically thick (100 nm); therefore, optical transmission can be neglected. The dimensions of nanostructure arrays are $300 \times 300\ \mu m^2$. The propagation direction and polarization of the illumination incident source are, respectively, along the z-axis and x-axis, as indicated in Figure 1a.

Scanning electron microscope (SEM) images of the fabricated gold nanowire and nanoring arrays are shown in Figure 2a,c. The spectral absorption (A) of these all-metallic arrays is defined by $1 - T - R$, where T and R represent the transmission and reflection from NBA samples. Optically thick (100 nm) gold film prevents light transmission and reduces the absorption to $1 - R$. Optical measurements are performed using an inverted optical microscope to obtain the reflection. Figure 2b,d plots the measured absorption spectra of the nanowire and nanoring arrays, which exhibit a pronounced sharp resonance peak. For the nanowire arrays, a narrow resonance peak is observed at 708 nm with the maximum extinction value of 30%, whereas for the nanorings, the maximum absorption is over 90% measured at 755 nm. The full width at half-maximum (fwhm) values of absorption resonances are measured to be 9 nm for nanowire arrays and 12 nm for nanoring arrays. The quality factors of these resonator arrays are

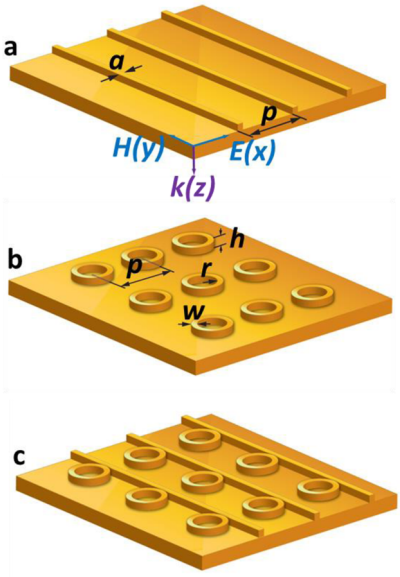

Figure 1. Schematic drawings of narrow band absorbers based on all-metallic nanostructure arrays. (a) Nanowire arrays deposited on gold film in the $x-y$ plane. The width of nanowire a is 100 nm with the lattice constant $p = 700$ nm. The illumination source propagates along the z-direction with E-field polarized along the x-axis, as illustrated in the figure. (b) Nanoring arrays. The inner radius of the nanoring, r, is 100 nm and its width, w, is 140 nm. The height of the nanoring, h, is 40 nm. The period of array, p, is 700 nm. (c) Nanoring/nanowire composite structure with the same geometrical parameters.

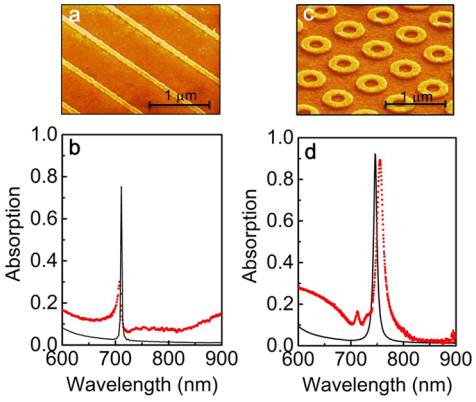

Figure 2. Narrow band absorber. (a) Scanning electron microscope images of the fabricated gold nanowire and (c) nanoring arrays on gold film. The inset scale bar is 1 μm. (b) Measured (red dots) and simulated (black curves) absorption spectra for nanowire and (d) nanoring arrays on gold film.

calculated to be 79 and 63, respectively, which is quite high for resonators comprising lossy metals. Three-dimensional finite-difference time-domain (FDTD) simulations were also performed using commercial software (Lumerical), and the corresponding absorption spectra for both nanowire and nanoring arrays are plotted in Figure 2b,d. In the simulations, complex optical constants for Au are taken from Palik.[25] Our numerical simulations predict the resonance wavelength of resonant absorbers; however, there is a slight

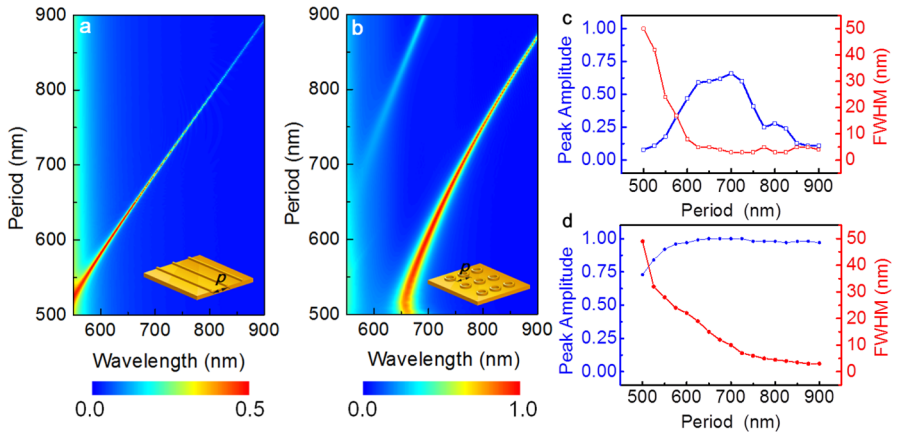

Figure 3. Flexibility of resonance wavelength, peak amplitude, and line width tuning for nanowire/nanoring arrays. (a) Absorption spectra plotted as a function of wavelength and period for nanowire and (b) nanoring arrays on a metallic substrate. (c) Peak amplitude and fwhm of absorption resonance as a function of the period of nanowire and (d) nanoring arrays.

mismatch in bandwidths and peak amplitudes that can be associated with the imperfections and surface roughness due to actual fabrication. Limited by the finite array size of fabricated samples, the far-field measurements can be performed over a finite acceptance angle, thus also broadening the NBA spectrum.

In order to better evaluate and understand the effect of geometrical parameters on the resonance absorption characteristics, we have performed additional FDTD simulations for nanowire and nanoring arrays with different periodicities. Absorption spectra for increasing periodicities are plotted in Figure 3a,b, indicating that the high absorption peak position strongly depends on the periodicity of the nanostructure arrays. Other geometric parameters of nanowire or nanoring arrays, including width, radius, and thickness of the nanostructures, are also investigated in simulations (the results are plotted in Supporting Information Figure S1). Our results indicate that the most significant factor in determining the resonance wavelength is the periodicity, while other parameters such as metal thickness, width, and the size of the nanostructures provide slight modification in the resonance wavelength.[26] However, these geometrical parameters could significantly change the absorption intensity as discussed in Supporting Information. SLRs can be identified for the NBA resonance because periodic effect typically yields narrow band resonance depending on the lattice constant.[27−30] However, SLRs are essentially intricate combinations of localized/delocalized surface plasmon resonances on diffractive orders in periodic arrays, not only determined by periodic effect but also influenced by the plasmonic nature of metallic structures. For nanowire arrays (Figure 3a), the resonance wavelength follows the periodicity and increases linearly with increased periodicity. On the other hand, the resonance wavelength of nanoring arrays (Figure 3b) deviates from the periodicity, and the resonance wavelength is modified by the shape and size of the nanoring structure. Particularly, the deviation of resonance wavelength from periodicity is far more considerable for nanorings placed in smaller periodicity, due to the stronger plasmonic coupling between adjacent nanorings when the unit cells are physically closer. Figure 3c,d plotted the peak amplitude and fwhm as a function of lattice constant of nanowire and nanoring arrays, respectively. For practical applications, it is desirable to have an optical ideal absorber with narrow band feature and high absorptivity amplitude. For the case of NBA based on nanowire arrays, the periodicity size of 700 nm is found to be an optimal case with the highest absorption amplitude of 66%. The fwhm is increasingly larger for smaller periodicities due to stronger coupling and higher filling factors of metal for each unit cell; however, by increasing the periodicity, one can reduce the coupling and thus the resonance bandwidth. For nanoring arrays, as periodicity is larger than 700 nm, the peak amplitude remains unchanged with nearly ideal absorption exceeding 97% and fwhm at 900 nm is calculated to be 3 nm. For larger lattice constants, nanoring arrays exhibit higher absorbance with reduced narrow bandwidth, therefore becoming more suitable for use in NBA applications when compared to conventional metallic stripes (nanowires). There is a wide range of parameter space for designing narrow band absorbers in which the resonance wavelength, the bandwidth, and the peak amplitude can be controlled to address the needs and specifications for desired applications.[31,32] Additionally, another obvious benefit of using nanoring arrays over nanowire arrays is that the absorption characteristics are polarization insensitive, whereas nanowires exhibit polarization-dependent absorption phenomena.

We have performed numerical three-dimensional (3D) simulations to calculate the spatial distribution of absorbed power inside NBA. Figure 4 displays the 2D/3D spatially absorbed power distribution for

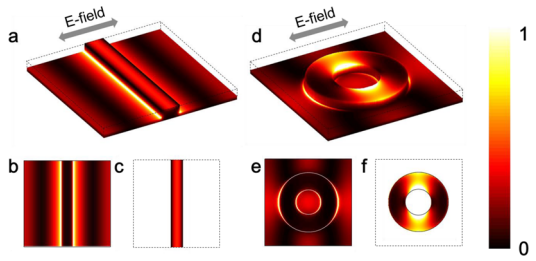

Figure 4. Absorbed power distribution maps in metal. (a) Three-dimensional absorbed power distribution map for the nanowire structure. (b) Two-dimensional absorbed power map for the nanowire at the interface of the bottom nanowire and metallic film at the resonance peak. (c) Two-dimensional absorbed power map for the nanowire at the top surface of the resonance peak. (d) Three-dimensional absorbed power distribution map for the nanoring structure. (e) Two-dimensional absorbed power map for the nanoring at the interface of the bottom nanoring and metallic film at the resonance peak. (f) Two-dimensional absorbed power map for the nanoring at the top surface of the resonance peak. The maximum color scale for d, e, and f is 2.5 times higher than that for a, b, and c.

nanowire/nanoring NBA structures. The appearance of the sharp spectral feature indicates that the metallic layer enables much stronger radiant coupling with the SLR,[33−35] as shown in Figure 4. Figure 4a,d plots 3D absorbed power contours for a single unit cell of nanowire and nanoring arrays. The highest absorbed power intensity is located around the nanostructures due to strong diffractive and plasmonic interactions at resonance wavelength, although the exact positions of the hotspots differ for both NBA designs. In order to clearly visualize the spatially absorbed power distribution, we plotted the 2D absorbed power contour at the interface of the metallic substrate and the bottom surface of the nanostructures (Figure 4b,e), as well as the interface of the top surface of nanostructures and air (Figure 4c,f). The maximum absorbed power for nanowires is located at the two sides of gratings and the interface between the bottom surface of nanowires and metallic film (Figure 4b), whereas the highest absorbed power for the nanoring arrays is located at the inner parts of rings and top surfaces (Figure 4f). Such distinctive absorption schemes for nanorings and nanowires are attributed to different SLR spectra in terms of NBA bandwidth and amplitude.

Nanostructures fabricated on metallic substrates have significant advantages over their counterparts fabricated on dielectric substrates. High reflective substrates underneath the nanostructures provide strong optical interaction and scatter light back into the air or the surface wave rather than forward into a dielectric medium. By eliminating such forward scattering, radiative losses are significantly reduced, contributing to the narrower absorption band observed in the experiments. All-metallic absorbers drive the electromagnetic (EM) field resonance away from substrate interface to the top surfaces of the nanostructure. The excited mode from the top surfaces could boost the local field enhancement to over three times higher than counterparts on dielectric medium (detailed discussions are provided in the Supporting Information Figure S4).[36] Overall, the highly excited SLR mode facilitated by the underneath metallic substrate contributes to sharp absorptivity and a much higher quality factor nanocavity, rather than a leaky mode cavity based on transparent substrate or MIM-type cavity.

The top surface field concentration and extension into surrounding medium for the all-metallic NBA is quite desirable for biosensing application due to the easy accessibility of the field.[9] The numerical simulations indicate that the sensitivity ($S = d\lambda/dn$) and figure of merit (FoM = $(d\lambda/dn)/\Delta\lambda$) for a plasmonic sensor to index variation could reach as high as ~900 and ~200, respectively. Such high FoM for sensing is due to ultranarrow bandwidth resonance and highly concentrated local field near the nanorings/nanowires. In addition to biosensing, spectrally ultrasharp bandwidth with nearly ideal absorptivity could have significant impact on applications including thermophotovoltaics and absorption filters.

Nanoring/Nanowire Hybrid System. We also investigate the hybrid system that consists of nanoring arrays incorporated with nanowires, as schematically illustrated in Figure 5a. Corresponding SEM images are shown in Figure 5d. The geometric parameters and the periodicity for the nanoring and nanowire arrays are kept the same as individual arrays discussed in the previous section. Here, we introduce structural asymmetry to the nanowire−nanoring composite structure, where the asymmetric extent is characterized by Δx, the displacement of the nanowire with respect to the center of the nanoring along the x-axis. The plasmonic couplings between the nanoring and nanowire change with Δx, due to hybridization between the two absorption resonances from the nanoring and nanowire arrays separately. As shown in Figure 5b,c, both measured and simulated data illustrate the appearance of resonance splitting due to symmetry breaking.[9,37,38] For a symmetric ring/wire system with $\Delta x = 0$ nm, only one pronounced resonance is located at 737 nm in the measured spectrum. Shifting the wire to Δx = ~200 nm, where the nanowires overlapped with nanorings, we experimentally observe the resonances are split into two coupled narrow band resonances located at 709 and 765 nm, respectively. For the ring/wire system with Δx = ~270 nm offset, where the nanoring and nanowire are conductively touching,[39] the two individual resonances slightly red shift in spectral response. Eventually, when the nanowires are shifted to the middle of adjacent nanorings (*i.e.*, $\Delta x = 350$ nm), the hybrid system is reverted to symmetry and the two split resonances are reduced to the original single peak. The simulated FDTD results could reproduce the same spectral evolution trends (Figure 5b) and have good agreement with measured spectra

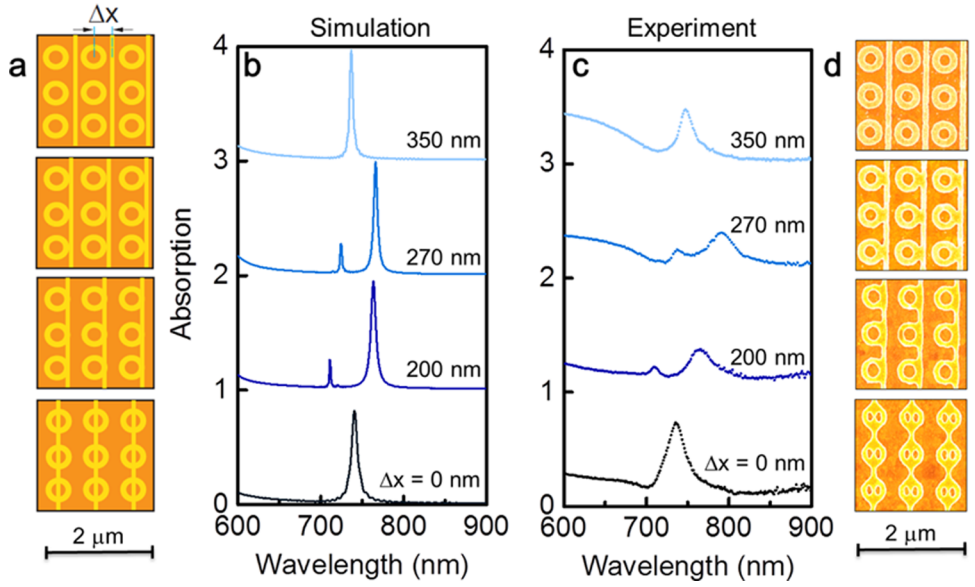

Figure 5. Spectral hybridization for nanoring/nanowire arrays. (a) Schematic configuration and (d) scanning electron microscope images for a top-view nanoring/nanowire hybrid system with different displacement of Δx = 0, 200, 270, and 350 nm. Scale bar is 2 μm. (b) Simulated and (c) measured absorptivity spectra for the nanoring/nanowire hybrid system with corresponding varied displacement Δx.

(Figure 5c). Reduced amplitude and broadening effect in experimental spectra are mainly attributed to surface roughness and deviation of fabricated structures from the ideal parameters.

To gain more insight on the resonance splitting effect from introducing asymmetric hybridization between nanorings and nanowires, complete spectral evolution as a function of asymmetric displacement Δx is numerically calculated. As illustrated in Figure 6a, two narrower absorption peaks arise from the original single absorption peak once symmetry breaking and more EM energy absorption is intensively concentrated in the resonance of longer wavelength due to larger absorptivity amplitude. Interestingly, we observe a drastic EM energy absorption peak transition region from 760 to 730 nm when the asymmetric ring/wire system with Δx = 290−320 nm is offset. It is worth noting that, within the specific displacement region, the nanoring and nanowire are nearly touching, which induces plasmonic capacitive coupling between their SLR modes.[40] For further displacement of Δx = 320−350 nm, increasingly higher EM energy absorbance is located in the shorter wavelength resonance, whereas the longer wavelength peak gradually disappears, eventually resulting in a single absorption peak.

We calculated the local electric field (E-field) intensity to understand the underlying physical mechanism of resonance coupling in the absorptivity spectra. Figure 6b presents the E-field profiles in the x−y plane across the center of the nanoring/nanowire structures for both individual nanostructured arrays as well as their hybrid system with different displacement of Δx at respective resonance peak. For the individual

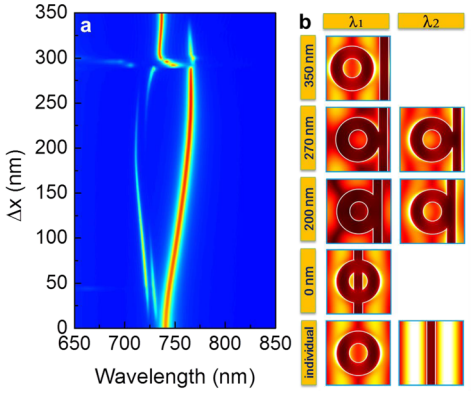

Figure 6. Absorption evolutions with displacement Δx variation and near E-field profile for the nanoring/nanowire hybrid system. (a) Absorptivity spectral evolution as a function of wavelength and displacement Δx in the nanowire−nanoring hybrid structure. (b) Normalized 2D E-field intensity distribution for the individual systems and hybrid system when Δx = 0, 200, 270, and 350 nm. The field monitor is located at the x−y plane across the center of the nanoring/nanowire structures at respective peak wavelengths.

systems (the bottom row of Figure 6b), both of the nanoring and nanowire exhibit a strong symmetric pattern of E-field intensity near the metallic structures. Similarly, for the hybrid system with Δx = 0 nm displacement, only one single resonance peak arises due to the symmetric mutual coupling, where the E-field distribution profile of the nanoring resonance dominates and overrides the contribution of the nanowire. For Δx = 200 nm, two resonance peaks at shorter wavelength λ_1 and longer wavelength λ_2 are induced by resonant coupling due to asymmetry, and higher E-field intensity at resonance λ_2 confirms that more EM

energy absorption is concentrated there. The E-field distribution pattern for $\Delta x = 200$ nm is not only dominated by the nanoring but also attributed to hybridization of the nanoring and nanowire since the field near the nanowire structures has high intensity. Similarly, for the nearly touching case of $\Delta x = 270$ nm, enhanced near-field density surrounds both the nanoring and the nanowire. However, the field pattern is different from the case of $\Delta x = 200$ nm in terms of field profile of shorter wavelength λ_1, which indicates drastic variation of the coupling mechanism due to the relative position change. Eventually, for $\Delta x = 350$ nm, when the nanoring is apart from the nanowire, the hybrid system returns to a symmetric pattern and there is minimal mutual coupling. The nanoring again dominates the surrounding field distribution and leads to the degeneration from two coupled resonances to a single absorption peak.

CONCLUSION

Narrow band absorbers are realized using periodic nanoring and nanowire arrays that are directly deposited on reflective metallic films. We observed ultrasharp absorption resonances with fwhm as narrow as 12 nm and absorption peak amplitude exceeding 90%. The narrow line width is obtained *via* surface lattice plasmon resonances. Therefore, the wavelength and the line width of absorption bands can be accessibly controlled with the periodicity and the shape of the nanostructures. We demonstrate that all-metallic resonant absorbers enable stronger light−matter interactions, as opposed to widely studied MIM absorbers, and exhibit higher E-field enhancement concentrated near the nanostructures. Realization of such resonant absorbers with ultranarrow bandwidth (∼10 nm) and nearly ideal absorptivity (>90%) has been challenging in the field of plasmonics. The NBA design is a promising scheme for achieving ultrasharp perfect absorption based on optical systems conventionally known to be very lossy. Such ultranarrow band resonant absorbers could easily find applications in thermophotovoltaics, optical filters, nonlinear optics, and biosensors, where spectrally ultranarrow optical resonances and large signals are desired.

METHODS

Fabrication. Cr/Au layers (5/100 nm thick) were first coated on silicon substrates using electron beam (E-beam) deposition. We used PMMA 990 A4 as the E-beam resist and spun it at 4000 rpm for 40 s. Consequently, the sample was baked at 180 °C for 90 s on a hot plate. E-beam lithography was conducted to define the patterns. The sample was developed in 1:3 methyl isobutyl ketone/isopropyl alcohol (IPA) solution followed by rinsing in IPA. Then 40 nm Au layers were deposited on the patterned substrates by E-beam evaporation. A lift-off process was performed by dipping the sample in acetone for 2 min, followed by a 10 s sonication process.

Optical Measurements. An inverted microscope equipped with a spectrometer consisting of a 303 mm focal length monochromator and Andor Newton electron multiplication charge-coupled device (EM-CCD) camera was utilized for optical measurements. A broad-band halogen lamp was used to generate a broad-band illumination, and a linear polarizer was inserted into the light pathway to polarize the incident light. Reflected light was collected from a 50 × 50 μm^2 area using a 2× Nikon microscope objective with a numerical aperture of 0.06. For calibration of reflection, we first measured the reflection from a broad-band dielectric mirror (Edmund Optics #64-114) with an average reflection of 99% between 350 and 1100 nm. Measured reflection from nanostructures was then calibrated using the reflection spectra of the dielectric mirror.

FDTD Simulations. Full-field electromagnetic wave calculations were performed using Lumerical, a commercially available FDTD simulation software package. A unit cell of the investigated structure was simulated using periodic boundary conditions along the *x*- and *y*-axes and perfectly matched layers along the propagation of electromagnetic waves (*z*-axis). Plane waves were launched incident to the unit cell along the +*z* direction, and reflection was collected with a power monitor placed behind the radiation source; transmission was collected with a power monitor placed behind the structure. Electric and magnetic field distribution were detected within the 3D field profile monitors. All of the simulations reported in this paper were performed in 3D layouts. In the simulations, we used Au Palik data for the complex refractive indices.[25]

Conflict of Interest: The authors declare no competing financial interest.

Acknowledgment. This material is based upon work supported by the AFOSR under Award No. FA9550-12-1-0280. K.A. acknowledges financial support from the McCormick School of Engineering and Applied Sciences at Northwestern University and partial support from the Institute for Sustainability and Energy at Northwestern (ISEN) through ISEN Equipment and Booster Awards. This research was also partially supported by the Materials Research Science and Engineering Center (NSF-MRSEC) (DMR-1121262) of Northwestern University. This research made use of the NUANCE Center at Northwestern University, which is supported by NSF-NSEC, NSF-MRSEC, Keck Foundation, and the State of Illinois and the NUFAB cleanroom facility at Northwestern University. We also thank Tuncay Ozel for technical help.

Supporting Information Available: Supplementary NBA spectrum of structural size investigation, field profiles, and sensitivity calculations for biochemical sensing applications. This material is available free of charge *via* the Internet at http://pubs.acs.org.

REFERENCES AND NOTES

1. Shalaev, V. M. Optical Negative-Index Metamaterials. *Nat. Photonics* **2007**, *1*, 41–48.
2. Valentine, J.; Zhang, S.; Zentgraf, T.; Ulin-Avila, E.; Genov, D. A.; Bartal, G.; Zhang, X. Three-Dimensional Optical Metamaterial with a Negative Refractive Index. *Nature* **2008**, *455*, 376–379.
3. Pendry, J. B. Negative Refraction Makes a Perfect Lens. *Phys. Rev. Lett.* **2000**, *85*, 3966.
4. Fang, N.; Lee, H.; Sun, C.; Zhang, X. Sub-Diffraction-Limited Optical Imaging with a Silver Superlens. *Science* **2005**, *308*, 534–537.
5. Schurig, D.; Mock, J.; Justice, B.; Cummer, S.; Pendry, J.; Starr, A.; Smith, D. Metamaterial Electromagnetic Cloak at Microwave Frequencies. *Science* **2006**, *314*, 977–980.
6. Ou, J.-Y.; Plum, E.; Jiang, L.; Zheludev, N. I. Reconfigurable Photonic Metamaterials. *Nano Lett.* **2011**, *11*, 2142–2144.

7. Pryce, I. M.; Kelaita, Y. A.; Aydin, K.; Atwater, H. A. Compliant Metamaterials for Resonantly Enhanced Infrared Absorption Spectroscopy and Refractive Index Sensing. *ACS Nano* **2011**, *5*, 8167–8174.
8. Chen, H.-T.; O'Hara, J. F.; Azad, A. K.; Taylor, A. J.; Averitt, R. D.; Shrekenhamer, D. B.; Padilla, W. J. Experimental Demonstration of Frequency-Agile Terahertz Metamaterials. *Nat. Photonics* **2008**, *2*, 295–298.
9. Cetin, A. E.; Altug, H. Fano Resonant Ring/Disk Plasmonic Nanocavities on Conducting Substrates for Advanced Biosensing. *ACS Nano* **2012**, *6*, 9989–9995.
10. Larsson, E. M.; Alegret, J.; Käll, M.; Sutherland, D. S. Sensing Characteristics of NIR Localized Surface Plasmon Resonances in Gold Nanorings for Application as Ultrasensitive Biosensors. *Nano Lett.* **2007**, *7*, 1256–1263.
11. Kabashin, A.; Evans, P.; Pastkovsky, S.; Hendren, W.; Wurtz, G.; Atkinson, R.; Pollard, R.; Podolskiy, V.; Zayats, A. Plasmonic Nanorod Metamaterials for Biosensing. *Nat. Mater.* **2009**, *8*, 867–871.
12. Offermans, P.; Schaafsma, M. C.; Rodriguez, S. R.; Zhang, Y.; Crego-Calama, M.; Brongersma, S. H.; Gómez Riva, J. Universal Scaling of the Figure of Merit of Plasmonic Sensors. *ACS Nano* **2011**, *5*, 5151–5157.
13. Aydin, K.; Ferry, V. E.; Briggs, R. M.; Atwater, H. A. Broadband Polarization-Independent Resonant Light Absorption Using Ultrathin Plasmonic Super Absorbers. *Nat. Commun.* **2011**, *2*, 517.
14. Narimanov, E. E.; Kildishev, A. V. Optical Black Hole: Broadband Omnidirectional Light Absorber. *Appl. Phys. Lett.* **2009**, *95*, 41106.
15. Hirsch, L. R.; Stafford, R.; Bankson, J.; Sershen, S.; Rivera, B.; Price, R.; Hazle, J.; Halas, N.; West, J. Nanoshell-Mediated Near-Infrared Thermal Therapy of Tumors under Magnetic Resonance Guidance. *Proc. Natl. Acad. Sci. U.S.A.* **2003**, *100*, 13549–13554.
16. Stipe, B. C.; Strand, T. C.; Poon, C. C.; Balamane, H.; Boone, T. D.; Katine, J. A.; Li, J.-L.; Rawat, V.; Nemoto, H.; Hirotsune, A. Magnetic Recording at 1.5 Pb m^{-2} Using an Integrated Plasmonic Antenna. *Nat. Photonics* **2010**, *4*, 484–488.
17. Knight, M. W.; Sobhani, H.; Nordlander, P.; Halas, N. J. Photodetection with Active Optical Antennas. *Science* **2011**, *332*, 702–704.
18. Liu, X.; Tyler, T.; Starr, T.; Starr, A. F.; Jokerst, N. M.; Padilla, W. J. Taming the Blackbody with Infrared Metamaterials as Selective Thermal Emitters. *Phys. Rev. Lett.* **2011**, *107*, 045901.
19. Liu, N.; Mesch, M.; Weiss, T.; Hentschel, M.; Giessen, H. Infrared Perfect Absorber and Its Application as Plasmonic Sensor. *Nano Lett.* **2010**, *10*, 2342–2348.
20. Neumann, O.; Urban, A. S.; Day, J.; Lal, S.; Nordlander, P.; Halas, N. J. Solar Vapor Generation Enabled by Nanoparticles. *ACS Nano* **2012**, *7*, 42–49.
21. Zhang, S.; Fan, W.; Panoiu, N.; Malloy, K.; Osgood, R.; Brueck, S. Experimental Demonstration of Near-Infrared Negative-Index Metamaterials. *Phys. Rev. Lett.* **2005**, *95*, 137404.
22. Soukoulis, C. M.; Wegener, M. Past Achievements and Future Challenges in the Development of Three-Dimensional Photonic Metamaterials. *Nat. Photonics* **2011**, *5*, 523–530.
23. Väkeväinen, A.; Moerland, R. J.; Rekola, H. T.; Eskelinen, A.-P.; Martikainen, J.-P.; Kim, D.-H.; Törmä, P. Plasmonic Surface Lattice Resonances at the Strong Coupling Regime. *Nano Lett.* **2014**, *14*, 1721–1727.
24. Zhou, W.; Odom, T. W. Tunable Subradiant Lattice Plasmons by Out-of-Plane Dipolar Interactions. *Nat. Nanotechnol.* **2011**, *6*, 423–427.
25. Palik, E. D. *Handbook of Optical Constants of Solids*; Academic: Orlando, FL, 1985.
26. Halpern, A. R.; Corn, R. M. Lithographically Patterned Electrodeposition of Gold, Silver, and Nickel Nanoring Arrays with Widely Tunable Near-Infrared Plasmonic Resonances. *ACS Nano* **2013**, *7*, 1755–1762.
27. Zou, S.; Janel, N.; Schatz, G. C. Silver Nanoparticle Array Structures That Produce Remarkably Narrow Plasmon Lineshapes. *J. Chem. Phys.* **2004**, *120*, 10871.
28. Hicks, E. M.; Zou, S.; Schatz, G. C.; Spears, K. G.; Van Duyne, R. P.; Gunnarsson, L.; Rindzevicius, T.; Kasemo, B.; Käll, M. Controlling Plasmon Line Shapes through Diffractive Coupling in Linear Arrays of Cylindrical Nanoparticles Fabricated by Electron Beam Lithography. *Nano Lett.* **2005**, *5*, 1065–1070.
29. Chu, Y.; Schonbrun, E.; Yang, T.; Crozier, K. B. Experimental Observation of Narrow Surface Plasmon Resonances in Gold Nanoparticle Arrays. *Appl. Phys. Lett.* **2008**, *93*, 181108.
30. Vecchi, G.; Giannini, V.; Rivas, J. G. Shaping the Fluorescent Emission by Lattice Resonances in Plasmonic Crystals of Nanoantennas. *Phys. Rev. Lett.* **2009**, *102*, 146807.
31. Zhang, J.; Ou, J.; MacDonald, K.; Zheludev, N. Optical Response of Plasmonic Relief Meta-Surfaces. *J. Opt.* **2012**, *14*, 114002.
32. Zhang, J.; Ou, J.-Y.; Papasimakis, N.; Chen, Y.; MacDonald, K. F.; Zheludev, N. I. Continuous Metal Plasmonic Frequency Selective Surfaces. *Opt. Express* **2011**, *19*, 23279–23285.
33. Carron, K.; Fluhr, W.; Meier, M.; Wokaun, A.; Lehmann, H. Resonances of Two-Dimensional Particle Gratings in Surface-Enhanced Raman Scattering. *J. Opt. Soc. Am. B* **1986**, *3*, 430–440.
34. Sobhani, A.; Knight, M. W.; Wang, Y.; Zheng, B.; King, N. S.; Brown, L. V.; Fang, Z.; Nordlander, P.; Halas, N. J. Narrowband Photodetection in the Near-Infrared with a Plasmon-Induced Hot Electron Device. *Nat. Commun.* **2013**, *4*, 1643.
35. Kravets, V.; Schedin, F.; Grigorenko, A. Extremely Narrow Plasmon Resonances Based on Diffraction Coupling of Localized Plasmons in Arrays of Metallic Nanoparticles. *Phys. Rev. Lett.* **2008**, *101*, 087403.
36. Fafarman, A. T.; Hong, S.-H.; Caglayan, H.; Ye, X.; Diroll, B. T.; Paik, T.; Engheta, N.; Murray, C. B.; Kagan, C. R. Chemically Tailored Dielectric-to-Metal Transition for the Design of Metamaterials from Nanoimprinted Colloidal Nanocrystals. *Nano Lett.* **2012**, *13*, 350–357.
37. Hao, F.; Sonnefraud, Y.; Dorpe, P. V.; Maier, S. A.; Halas, N. J.; Nordlander, P. Symmetry Breaking in Plasmonic Nanocavities: Subradiant LSPR Sensing and a Tunable Fano Resonance. *Nano Lett.* **2008**, *8*, 3983–3988.
38. Francescato, Y.; Giannini, V.; Maier, S. A. Plasmonic Systems Unveiled by Fano Resonances. *ACS Nano* **2012**, *6*, 1830–1838.
39. Hao, F.; Nordlander, P.; Burnett, M. T.; Maier, S. A. Enhanced Tunability and Linewidth Sharpening of Plasmon Resonances in Hybridized Metallic Ring/Disk Nanocavities. *Phys. Rev. B* **2007**, *76*, 245417.
40. Rodriguez, S. R. K.; Abass, A.; Maes, B.; Janssen, O. T.; Vecchi, G.; Rivas, J. G. Coupling Bright and Dark Plasmonic Lattice Resonances. *Phys. Rev. X* **2011**, *1*, 021019.